Acta Neuropathol (2006) 112:287–303
DOI 10.1007/s00401-006-0085-5

ORIGINAL PAPER

Minicolumnar abnormalities in autism

Manuel F. Casanova · Imke A. J. van Kooten · Andrew E. Switala · Herman van Engeland · Helmut Heinsen · Harry W. M. Steinbusch · Patrick R. Hof · Juan Trippe · Janet Stone · Christoph Schmitz

Received: 28 March 2006 / Revised: 9 May 2006 / Accepted: 10 May 2006 / Published online: 4 July 2006

Abstract Autism is characterized by qualitative abnormalities in behavior and higher order cognitive functions. Minicolumnar irregularities observed in autism provide a neurologically sound localization to observed clinical and anatomical abnormalities. This study corroborates the initial reports of a minicolumnopathy in autism within an independent sample. The patient population consisted of six age-matched pairs of patients (DSM-IV-TR and ADI-R diagnosed) and controls. Digital micrographs were taken from cortical areas S1, 4, 9, and 17. The image analysis produced estimates of minicolumnar width (CW), mean interneuronal distance, variability in CW (V_{CW}), cross section of Nissl-stained somata, boundary length of stained somata per unit area, and the planar convexity. On average CW was 27.2 μm in controls and 25.7 μm in autistic patients ($P = 0.0234$). Mean neuron and nucleolar cross sections were found to be smaller in autistic cases compared to controls, while neuron density in autism exceeded the comparison group by 23%. Analysis of inter- and intracluster distances of a Delaunay triangulation suggests that the increased cell density is the result of a greater number of minicolumns, otherwise the number of cells per minicolumns appears normal. A reduction in both somatic and nucleolar cross sections could reflect a bias towards shorter connecting fibers, which favors local computation at the expense of inter-areal and callosal connectivity.

Keywords Autistic disorder/pathology · Child development disorders · Pervasive · Neocortex · Neuropil · Pyramidal cells

M. F. Casanova (✉)
Department of Psychiatry and Behavioral Sciences,
University of Louisville, 500 South Preston St Bldg
55A Ste 217, Louisville, KY 40292, USA
e-mail: m0casa02@gwise.louisville.edu

I. A. J. van Kooten · H. van Engeland
Department of Child and Adolescent Psychiatry,
University Medical Center, Utrecht, The Netherlands

A. E. Switala · J. Trippe · J. Stone
Department of Psychiatry and Behavioral Sciences,
University of Louisville, Louisville, KY, USA

H. W. M. Steinbusch · C. Schmitz · I. A. J. van Kooten
Department of Psychiatry and Neuropsychology,
Division of Cellular Neuroscience, Maastricht University,
and European Graduate School of Neuroscience
(EURON), Maastricht, The Netherlands

H. Heinsen
Morphologic Brain Research Unit, University of Würzburg,
Würzburg, Germany

P. R. Hof
Department of Neuroscience,
Mount Sinai School of Medicine, New York, NY, USA

Introduction

Minicolumns are basic architectonic and physiological elements identified in all regions of the neocortex [16] and in all mammalian species thus far evaluated [37]. The minicolumnar circuit is an evolutionarily and ontogenetically conserved template adapted in the various cortical areas according to their specific developmental and functional requirements. The minicolumnar core comprises radially oriented arrays of pyramidal projection neurons. At the core and periph-

ery of the minicolumn, combinations of GABAergic interneurons provide for a diversity of signaling properties that serve to dynamically modulate pyramidal cell inputs and outputs that perform area and task-specific information processing needs [22, 30, 38, 51].

Available neuropathological and structural imaging data suggest that autism is the result of a developmental lesion capable of affecting brain growth. One possible explanation for this is the recent finding of minicolumnar abnormalities in autism (i.e., minicolumns of reduced size and increased numbers) [20]. In this initial study measures of minicolumnar morphometry were obtained relative to pyramidal cell arrays in nine autistic cases and in an equal number of controls. The feature extraction properties of the algorithms were corrected for minicolumnar fragments, curvature of the tissue section, and 3D proportions (stereological modeling) [24]. Later on, the same patient population was used to confirm the presence of cortical radial abnormalities in a study using the gray level index (GLI), i.e., proportional area covered by Nissl-stained to unstained elements in postmortem samples [21]. Other studies have provided evidence that the minicolumnar alterations in autism are not a nonspecific effect of mental retardation. Investigators have found that minicolumnar width in Down syndrome patients reaches adult proportions earlier than normal, possibly as a result of accelerated aging [16, 17]. In these studies minicolumnar size was reported to be normal despite the small brain size of Down syndrome patients.

An increase in the number of minicolumns is thought to underlie the neocortical expansion accompanying human encephalization, i.e., the process by which the brain has increased in size to a degree greater than expected when taking body size into account [88]. Empirical evidence and theoretical models indicate that local circuit neurons increase in number, complexity, and proportion relative to projection neurons during primate encephalization [45, 86]. These trends reflect the emergence in primates of a distinct population of dorsal telencephalic-derived inhibitory interneurons [59] modulating activity of minicolumnar pyramidal cells. Furthermore, isocortical areas such as dorsolateral prefrontal cortex, lacking direct homologs in non-primates, contain a well-defined granule cell layer of excitatory interneurons and increased numbers of supragranular local projection neurons [80]. Multiple polymorphisms associated with autism may be a consequence of phylogenetically recent changes in genetic programs guiding the development of species-specific cytoarchitectonic features. The morphometric analysis of such features complements genetic analysis. This study therefore investigates minicolumnopathy in an independent sample of autistic patients. It also expands on previous findings by studying cortical cell size and density as related to pyramidal cell arrays. The changes in these parameters, early during development, would provide for basic alterations in cortico-cortical connections and information processing.

Materials and methods

Clinical dataset

The diagnosis for each autistic patient was established postmortem by the Autism Tissue Program (ATP). A certified rater and trainer arranged for a postmortem visit with the family to obtain, with written consent, medical and clinical information via a questionnaire that included the Autism Diagnostic Interview-Revised (ADI-R; [63]).

The Harvard Brain Tissue Resource Center (HBTRC) questionnaire was modified to include autism-specific questions for ATP use. The information obtained included: donor and respondent identifying information; ethnicity, handedness and known exposure to hazardous materials; diagnostic information including dates and physician; genetic tests; pre- and postnatal medical history; immunization, medication, and hospitalization information; family history and additional information about donor participation in any training or research studies such as imaging, medication trials, and/or genetic studies. The supporting documents such as autopsy reports, death certificates, medical, clinical, and/or educational records were obtained at the time of the home visit or by sending written requests, signed by the legal next-of-kin, to named providers.

Brain specimens

Postmortem brains (one hemisphere per case) from six autistic cases (mean interval between death and autopsy 20.0 ± 2.9 h) and from six age-matched controls (mean interval between death and autopsy 24.0 ± 11.1 h) were analyzed (Table 1). Brains were obtained from several brain banks in the USA and Germany (see Acknowledgments). All autistic patients met the DSM-IV-TR [2] and ADI-R [62] criteria for autism. None of them exhibited any chromosomal abnormalities. In all of the cases, autopsy was performed after informed consent was obtained from a relative. The use of these autopsy cases was approved by the relevant Institutional Review Boards. Clinical records were available for all cases (see Appendix).

Table 1 Clinical characteristics of the cases included in this study

Patient	Sex	Hemisphere	Age (y)	Cause of death	Clinical history	History of seizures	Medication history	Brain weight (g)	PMI (h)	Section thickness (μm)
A1	M	L	4	Drowning	Asthma/bronchitis	No	Daily medication (not specified) for asthma/bronchitis	1,160	30	200
C1	M	L	4	Myocardial infarct—Takayasu arteritis	NH	NH	NH	1,380	5	500
A2	F	L	5	Car accident	Ear infections	No	Antibiotics for ear infections	1,390	13	200
C2	F	R	4	Lymphocytic myocarditis	NH	NH	NH	1,222	21	200
A3	M	R	8	Sarcoma	Syndactyly of the fingers and feet; colitis; high fever; neutropenia; metastatic alveolar rhabdomyosarcoma; large paravertebral mass extending from chest cavity to abdomen	Abnormal EEG; not diagnosed with seizure disorder	Depakote (1 year after EEG); chemotherapy; Peridex; Nystatin; GCSF; Benadryl; Pheergan; Dexamethasone; Morphine	1,570	22	200
C3	F	R	7	Status asthmaticus	NH	NH	NH	1,350	78	500
A4	M	L	13	Seizures	Severe hypotonia; ketogenic diet for 1.5 years	Yes	Dilatin (seizures); Anticonvulsants; Trileptal (seizures); Trazadone (sleep)	1,420	26	200
C4	M	R	14	Electrocution	NH	NH	NH	1,600	20	200
A5	F	R	20	Obstructive pulmonary disease	ADHD; microcephaly; epilepsy; schizophrenia	Yes (3 times)	Various psychotropic medications including Haldol, Ritalin, and Congentin; DepoProvera (birth control); Mellaril (sleep); Zoloft	1,108	15	200
C5	M	R	23	Ruptured spleen	NH	NH	NH	1,520	6	200
A6	M	R	24	Drowning	Pneumonia; bronchitis; behavioral problems	First seizure prior to death	Quetiapine (200 mg BID); Propanolol (400 mg BID); Thioridazine (50 mg HS)	1,610	14	200
C6	M	R	25	Cardiac tamponade	NH	NH	NH	1,388	14	500

A autism, *C* control, *M* male, *F* female, *L* left, *R* right, *NH* no history, *BW* brain weight, *PMI* postmortem interval, *y* years, *h* hours

Tissue processing

After immersion-fixation in 10% formalin for at least 3 months all hemispheres were mounted with celloidin and cut into entire series of 200-μm-thick coronal sections as described in detail elsewhere [43]. Three hemispheres were cut at 500-μm thickness. These differences did not influence the results of this study, since imaging of the tissue was done at high magnification, with a depth of field much narrower than 200 μm (see below, Image capture). Every third section (in one hemisphere: every second) was stained with gallocyanin.

Brain regions

Gallocyanin-stained sections were used by three of us (van Kooten, Heinsen, and Schmitz) to identify cortical areas M1, V1, frontal association cortex, and S1 (areas 4, 17, and 9 of Brodmann [13] and area 3b of Vogt and Vogt [101], respectively) according to anatomical landmarks and cytoarchitectural criteria (Fig. 1). Gross anatomical landmarks for M1 include the anterior wall of the central sulcus and adjacent portions of the precentral gyrus. Cytoarchitectonically, the region is clearly demarcated by its giant Betz cells and minimization of layer IV [89]. Area 17 (V1) is located along the walls of the calcarine sulcus in the occipital lobe and adjacent portions of the cuneus and lingual gyrus [19]. It is defined histologically by a broad lamina IV divided into three sublayers with numerous very small pyramidal cells in layers II and III. It is noted for the dense line of Gennari in myelin stains. Area 9 lies in the superior and middle frontal gyrus. Rajkowska and Goldman-Rakic [83, 84] found that it was located in the middle third of the superior frontal gyrus in all the cases they examined. It covered both dorsolateral and dorsomedial surfaces of the gyrus and extended, in some cases, to the depth of the superior frontal gyrus and portions of the middle frontal gyrus.

Fig. 1 Primary sensory cortex of an 8-year-old autistic male. Automatic segmentation has classified pixels as background, shown in *black*, and neurons, in *gray scale*. Clumps of neurons have been further separated into individual objects using the morphological watershed transform

Image capture

Regions of interest were delineated with a stereology workstation, consisting of a modified BX50 light microscope with UPlanApo objectives (Olympus, Tokyo, Japan), motorized specimen stage for automatic sampling (Ludl Electronics, Hawthorne, NY, USA), HV-C20AMP CCD color video camera (Hitachi, Tokyo, Japan), and StereoInvestigator software (MicroBrightField, Williston, VT, USA). Delineations were performed with a 10× objective (NA = 0.40). Digital micrographs each measuring about 200 μm by 150 μm were produced using the stereology workstation described above and a 40× oil objective (NA = 1.0). A few hundred such images were captured per region of interest to cover the entire cortical thickness. These images were assembled into one mosaic using the Virtual Slice module of the StereoInvestigator software. Only slight adjustments of contrast and brightness were made, without altering the data of the original materials.

Depth of field d_{tot} of the mosaic component images can be computed according to the formula

$$d_{\mathrm{tot}} = \left(\frac{\lambda}{\mathrm{NA}} + \frac{e}{M}\right) \times \frac{n}{\mathrm{NA}},$$

where λ is the wavelength of the illumination, M is the magnification, e is the resolution of the CCD (twice the distance between detectors), and n is the refractive index of the medium. These last two were $e = 16.2$ μm for the HV-C20AMP camera and $n = 1.5$ for oil. Taking λ on the order of 1 μm, d_{tot} was equal to about 2.1 μm, so images represent only a small virtual slice of the 200- or 500-μm-thick sections, and differences in section thickness were thus not considered as a confound.

Computerized image analysis

Multiple techniques reduced the images to sets of descriptive parameters. The minicolumn fragment

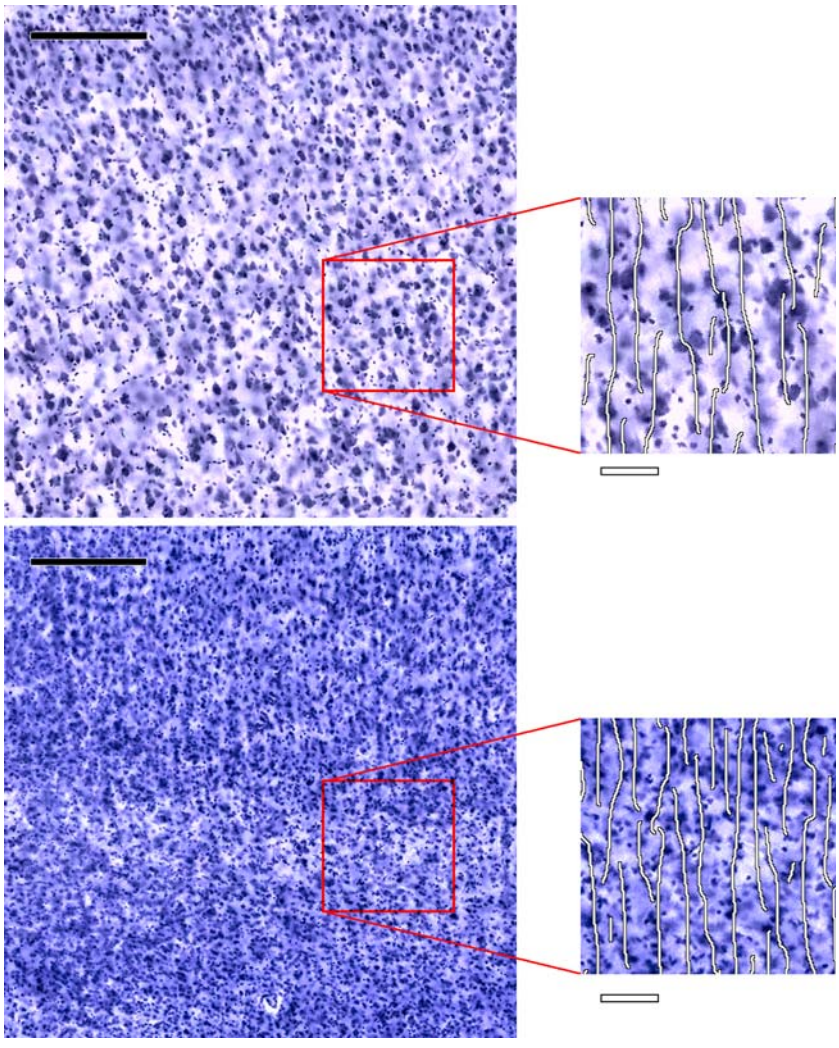

Fig. 2 Minicolumns in Brodmann area 4, lamina III, in an autistic patient (*bottom*) and an age-matched control case (*top*). *Insets* highlight the cores of minicolumn fragments identified by our software, illustrating the reduction in minicolumnar width (CW). *Scale bars* measure 200 μm on *left* and 50 μm on *right*

method [24] produced estimates of the mean width (CW) of minicolumns in a region of interest, the relative deviation (V_{CW}) of minicolumnar widths about the mean, and the mean distance (MCS) between neighboring neurons within the same minicolumn fragment (the ''CW'' and ''MCS'' notation being used for consistency with earlier publications [20]). The parameters mean grain size $(\bar{A})$, mean grain perimeter $(\bar{U})$, and intensity (λ) of a Boolean spatial model [99] were fit to each image. The GLI method [91, 92] reported the mean (D) and standard deviation (sd_D) of distances between ridges of high stain intensity, mean (W) and standard deviation (sd_W) of the width of these ridges, and their average height (A) above background. Lastly, the distribution of distances between neighboring neurons within each image was modeled as a mixture of two distributions with means (m_{near} and m_{far}) and standard deviations (s_{near} and s_{far}, respectively) with $m_{near} < m_{far}$. Details of each of the four methods are outlined below.

Computerized image analysis of minicolumnar structure in laminae II through VI was performed with algorithms described in the literature [24]. The feature extraction properties of the program were corrected for minicolumnar fragments, curvature of the tissue section, and have been adapted to 3D proportions (stereological modeling). The resulting estimates of minicolumnar width have also been validated against physiological measurements using intrinsic optical signaling and against anatomical measurements using myelinated fiber bundles [24].

Color mosaics were converted to intensity images and adaptively thresholded using a scale space approach [58]. Overlapping objects in the thresholded images were further separated using the watershed transformation. Each connected region in the resulting image was further classified according to size. Objects smaller than 10 μm^2, assumed to be glia, neuron fragments, or noise, were discarded altogether. Of the remaining objects, those with areas above the 15th

percentile were used for minicolumn fragment detection, while the smaller objects were classified as interneurons based on the fraction of all neurons estimated to be inhibitory by Braitenberg and Schüz [12].

Local neuron density was computed as the sum of equal contributions from large objects above the 15th percentile in the cross section. Each large neuron produced a density hump, peaking at the object's centroid, with elliptical contours oriented so that the major axes were parallel to the local radial direction, i.e. along the axis of the minicolumn, at each point in an image. The ridges in the neuronal density indicated the cores of minicolumn fragments, and objects including those classified as interneurons were parcellated into clusters according to the nearest fragment core. The average distance between neighboring fragment cores was addressed as the minicolumnar width CW (Fig. 2). Standard deviation of the logarithm of these distances was the scale-independent measure variability in minicolumn width (V_{CW}). Interneuronal distance (MCS) was the average distance between centroids of neighboring neurons within the same fragment. Only those fragments with more than ten neurons were considered when computing the means and standard deviations.

From the adaptively thresholded images, computerized image analysis produced estimates of the relative amount of area occupied by Nissl-stained tissue (A_A), the total boundary length of stained tissue per unit area (L_A), and the planar convexity (N_A^+); these quantities are of no interest in themselves but suffice to compute the parameters of a Boolean model with convex primary grains using the method of moments [99]. Each realization of the Boolean model is the union of a number of convex random closed sets (grains)—independently and identically distributed with mean area $\bar{A}$ and mean perimeter $\bar{U}$—located, or centered, at the points of a Poisson process with intensity λ. These three parameters, which completely determine the model, were obtained algebraically from the following equations [99], substituting for A_A, L_A, and N_A^+ their respective estimates:

$$A_A = 1 - e^{-\lambda \bar{A}},$$
$$N_A^+ = \lambda(1 - A_A),$$
$$L_A = N_A^+ \bar{U}.$$

Considering that the foreground pixels of a thresholded image correspond to locations in the original image overlapped by one or more stained cell soma, $\bar{A}$ is the average area of a neuronal cross section and λ is their density, i.e. number of neuronal cross sections per unit area. This technique was used to obtain these values without any need to segment individual neurons. The method of minicolumn fragments, on the other hand, does attempt to segment individual cell somata but uses the size of segmented objects only to sort them into size classes as described above.

Thresholded images were also analyzed according to the GLI method [91, 92], slightly modified so that the GLI would vary smoothly across a region (Figs. 3, 4).

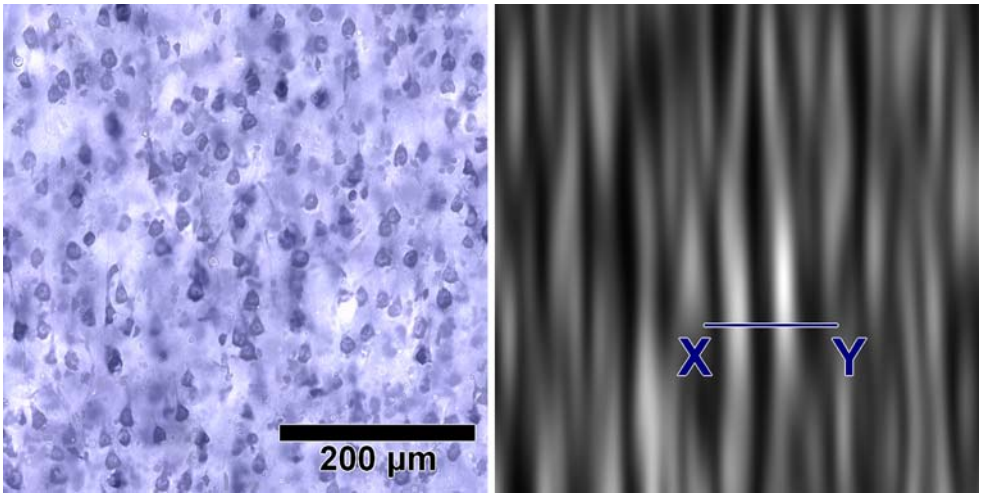

Fig. 3 *Left*: A 0.5 mm × 0.5 mm field from normal human primary motor cortex, lamina III. *Right*: Local GLI in the vicinity of each point in the field. Values are shown in *gray scale* from 1% (*black*) to 70% (*white*). For the significance of points *X* and *Y*, see Fig. 4. The gray level profile in this figure differs qualitatively from the example in Schleicher and Zilles [91] because we estimated GLI with a smooth, bell-shaped kernel and did not subsample the image. This allows for better localization of gray level peaks and troughs

Here, the inverse thresholded image, with foreground set equal to one and background set equal to zero, was convolved with a kernel measuring 11 μm by 110 μm at half-maximum. The long axis of the kernel was parallel to the axes of the minicolumns, assumed to be the image *Y*-axis. The result was an estimate of the GLI, or staining intensity, in the neighborhood of each pixel (Fig. 3). Each GLI image so produced was measured in profiles in the *X* direction to obtain the following parameters: (1) mean (*D*) and (2) standard deviation (sd_D) in the distance between local maxima of the GLI, (3) amplitude (*A*) of the local maxima, or difference between peak GLI and the lowest GLI between the peak in question and the next peak in the profile, and (4) mean (*W*) and (v) standard deviation (sd_W) in the width, i.e. full width to half maximum, of the peaks (Fig. 4).

A follow-up study considered the distance between neighboring objects. The objects were those classified as large neurons for the purposes of minicolumnar analysis (see above). Neurons were considered neighbors if (a) they were endpoints of an edge of the Delaunay triangulation of object centroids (Fig. 5), and (b) they were not further apart than the distance from either of them to the edge of the region of interest. Criterion (a) is equivalent to the geometric statement that three neurons are neighbors if the circle drawn through their centroids does not enclose the centroid of any other neuron. The criterion (b) is necessary to correct for a boundary effect where distant neurons are incorrectly labeled as neighbors because the true neighbors of one or more of them lie outside the region of interest. Now given that objects in a single lamina were clustered, as cells in minicolumns, an object's neighbors may include the members of the same cluster or the members of a nearby cluster (Fig. 6). Accordingly, the distribution of distances between neighbors (*d*) would then be a mixture of intracluster or near distances, and intercluster or far distances. This was modeled as a two-component log-normal mixture distribution; that is to say, the log *d* were assumed to be drawn from either of two Gaussian distributions of near and far distances:

$$\log d \sim \alpha N\left(\mu_{\text{near}}, \sigma^2_{\text{near}}\right) + (1-\alpha)N\left(\mu_{\text{far}}, \sigma^2_{\text{far}}\right);\ 0 \le \alpha \le 1.$$

Nucleolar size

Nucleoli were identified visually in digitized images. Twelve random locations were selected, per mosaic, by computer. The user identified the nucleolus nearest to each random point, excepting those points that did not fall within laminae II through VI. Nucleoli were segmented from the surrounding cytoplasm by thresholding according to Otsu's [73] method. If the thresholded nucleolus appeared to touch another object, the user manually removed pixels from that object until the nucleolus was separate. Nucleolar cross sections were measured by counting pixels in the thresholded nucleoli.

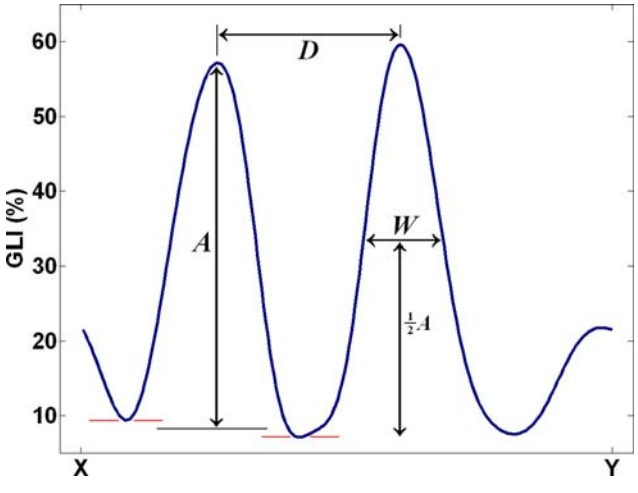

Fig. 4 GLI parameters are illustrated on a profile from points *X* to *Y* in Fig. 3: amplitude *A*, the difference between peak GLI and average trough GLI, distance *D* between peaks, and full width at half amplitude *W*

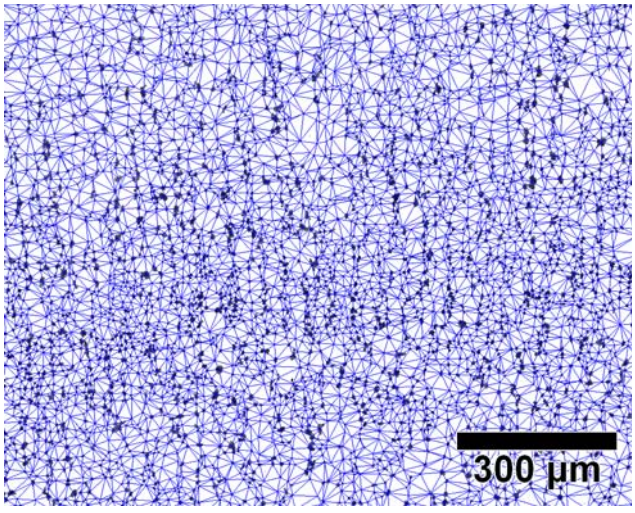

Fig. 5 Delaunay triangulation of larger neurons (*gray scale*) in the primary sensory cortex of an 8-year-old autistic male. Given a point set in the plane, neuron centroids in this case, the Delaunay triangulation is defined such that three points form the vertices of a *triangle* if and only if the *circle* through those points has no point from the set in its interior

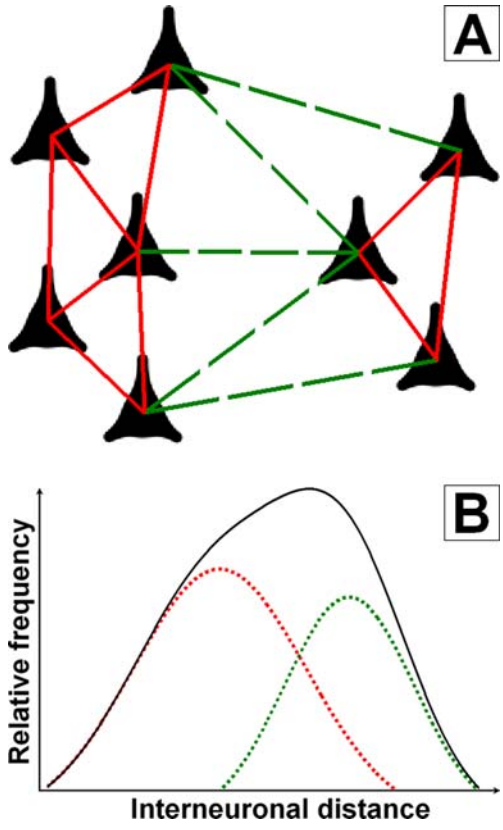

Fig. 6 **a** Owing to the clustering of neurons within minicolumns, the triangulation will include edges between objects in the same cluster (*solid lines*) and edges between objects in other clusters (*dotted lines*). The distribution of edge lengths over the whole graph will be a mixture of these two subgraphs' distributions. **b** We have estimated the locations and scales of distances within and between clusters by modeling the logarithm of edge lengths as a two-component Gaussian mixture (see text for details)

Statistical analysis

Autistic and control cases were sorted into age-matched pairs for the purposes of statistical analysis. Wilcoxon signed-rank tests were used to verify the absence of pairwise differences in brain weight or postmortem interval. Both tests were insignificant with $P = 0.84$. Otherwise, statistical analysis for all measurements employed repeated measures analysis of variance. Case pair (1–6) was the random factor, and fixed factors included diagnosis, sex, cortical area, and hemisphere. Interactions of the main effects involving both sex and cerebral hemisphere were excluded from the model due to multicolinearity. For the minicolumn fragment data only, a follow-up test was performed using a second model comprising the original model plus a factor for cortical lamina: III or V/VI. The model fitting and inferential statistics were performed with Matlab (The MathWorks, Natick, MA, USA).

Results

Minicolumnar width (CW) was greater in controls than in autistic persons by 1.46 μm or 5.54% of the mean [Student $t = 2.466$ with 19 degrees of freedom (*df*); $P = 0.0234$] (Table 2). CW also varied with cortical area ($F = 17.50$ with 3 numerator *df* and 19 denominator *df*; $P < 0.0001$), but no other effects were statistically significant. MCS exhibited a sex dependence in that the difference between control and autistic cases was greater in females than in males ($t = 2.227$ with 19 *df*; $P = 0.0382$); mean MCS was 18.3 and 18.9 μm in autistic females and males, respectively, and 19.7 and 18.6 μm in normal females and males, respectively. Again the only other significant effect was cortical area ($F = 16.09$ with 3 numerator *df* and 19 denominator *df*; $P < 0.0001$) (Table 2). There were no significant findings in V_{CW}. The follow-up analysis on those minicolumn fragments lying outside of lamina IV, using the supplemental model with lamina included as a factor, found no significant dependence of any measurement on lamina or lamina by diagnosis interaction.

Simultaneous multivariate analysis of neuron density and neuron profile area and perimeter (Table 3) revealed significant diagnosis dependence ($F = 5.47$ with 3 numerator *df* and 17 denominator *df*; $P = 0.0081$) and diagnosis by cortical area interaction ($F = 3.65$ with 9 numerator *df* and 41.5 denominator *df*; $P = 0.0020$). Mean particle cross section was 30.5 μm^2 less in autistic cases compared to controls ($t = 3.804$ with 19 *df*, $P = 0.0012$), while particle density was greater in autism: 5.15×10^3 mm^{-2} versus 4.19×10^3 mm^{-2} in controls ($t = -2.723$ with 19 *df*; $P = 0.0135$).

Each GLI parameter (Table 4) was reduced in autism: *D* by 1.93 μm ($t = 2.8465$ with 19 *df*; $P = 0.0103$), sd_D by 0.96 μm ($t = 2.1402$ with 19 *df*; $P = 0.0455$), *A*

Table 2 Average minicolumnar morphometry, broken down by diagnosis and cortical area

Area	CW (μm)		MCS (μm)		V_{CW} (%)	
	Autistic	Control	Autistic	Control	Autistic	Control
3	25.8	27.0	18.4	18.7	15.1	14.8
4	27.5	28.2	19.9	20.0	14.2	14.6
9	26.5	29.4	19.1	20.7	15.0	14.9
17	23.0	24.1	17.0	17.3	14.4	14.7
sd	1.2		0.8		0.9	

Scale-independent variation in minicolumnar width V_{CW} is expressed as percentage of the mean

CW minicolumnar width; *MCS* mean cell spacing (interneuronal distance); V_{CW} variability in minicolumnar distance; *sd* within-group standard deviation

Table 3 Estimated Boolean spatial model parameters of the texture of Nissl-stained material from each cortical area examined, in autistic and control individuals

	Area	$(\bar{A})(\mu m^2)$	$\bar{U}$ (μm)	λ (μm^{-2})
Autistic	3	128.0	44.2	0.0047
	4	144.9	45.7	0.0047
	9	131.9	44.5	0.0051
	17	114.8	44.8	0.0062
Control	3	151.1	49.4	0.0042
	4	154.7	48.3	0.0043
	9	182.3	51.8	0.0038
	17	153.4	53.3	0.0045
Standard deviation (within groups)		13.0	2.8	0.0008

$(\bar{A})$, mean soma cross section; $\bar{U}$, mean soma perimeter; λ, neuronal density

Table 4 Inhomogeneities in the gray level index, broken down by diagnosis and cortical area

	Area	A (%)	D (μm)	W (μm)	sd_D (μm)	sd_W (μm)
Autistic	3	16.0	32.1	15.2	13.1	6.1
	4	18.2	33.7	16.2	13.5	6.5
	9	16.9	32.3	15.4	12.8	5.9
	17	13.4	29.0	14.1	10.9	5.0
Control	3	17.4	33.3	15.8	13.5	6.3
	4	19.1	35.2	16.7	14.3	7.0
	9	19.2	35.0	16.7	14.0	6.8
	17	17.7	31.3	15.1	12.4	5.8
Standard deviation (within groups)		1.9	1.3	0.6	0.9	0.5

A, peak GLI above background; D, mean distance between peaks; W, mean peak width; sd_D, standard deviation of distance between peaks; sd_W, standard deviation of peak width

by 2.2% ($t = 2.226$ with 19 *df*; $P = 0.0383$), W by 0.86 μm ($t = 2.6936$ with 19 *df*; $P = 0.0144$), and sd_W by 0.59 μm ($t = 2.2643$ with 19 *df*; $P = 0.0354$).

Multivariate ANOVA, with dependent variable being the estimated mean logarithmic neighbor distances μ_{near} and μ_{far} (Table 5), found the diagnosis effect significant ($F = 3.72$ with 2 numerator *df* and 18 denominator *df*; $P = 0.044$). Near distances in autistic cases, averaged across all four areas, were 98.0% of those of controls [confidence interval (94.8%,101.0%)], and far distances were 94.8% of those of the normal comparison group [confidence interval (93.0%, 96.7%)]. Diagnosis by cortical area interaction was statistically insignificant.

Nucleolar cross sections (Table 6) were converted to radii of circles with the same area (r_{equiv}) in order to stabilize the variance for statistical analysis. Univariate ANOVA of mean (within each mosaic) r_{equiv}, again with the same model, revealed significant differences between autism and normal patients ($F = 19.52$ with 1 numerator and 17 denominator *df*; $P = 0.0004$). While r_{equiv} varied with cortical area ($F = 5.28$ with 3 numerator and 17 denominator *df*; $P = 0.0093$), there was no significant interaction with diagnostic group ($F = 0.89$ with 3 numerator and 17 denominator *df*; $P = 0.465$).

Discussion

The results of this study indicate that, within a limited brain sample, minicolumnar morphometry varies according to cortical region. Since traditional parcellation schemes have relied on subjective appraisals, the semi automated method used in this study may offer a rapid and accurate procedure to define cytoarchitectural brain regions. Results also corroborate a reduction in the width of minicolumns in the brains of autistic patients, using two different methods: one that measures pyramidal cell arrays [24] and another using the GLI [91, 92]. The Wilcoxon signed-rank test indicated essentially no (monotonic) difference between autistic patients and controls with respect to brain weight ($P = 0.84$) or postmortem interval ($P = 0.84$). The statistical design for all analyses included sex and cerebral hemisphere as fixed factors. Statistically significant, diagnosis-dependent differences between groups correspond, therefore, to the effect of diagnostic category independent of those other factors.

Given the lack of significant differences in brain weights between our comparison groups (Table 1), a generalized reduction in minicolumnar width in the autistic patients suggests their increase in total numbers. Although minicolumnar width was measured as distance between cell arrays in both the present and previous studies, differences in section thickness, tissue processing, and microscope objectives prevent us from making absolute comparisons. The feature extraction routines of our algorithms measure vertical clusters of neuronal profiles whose axis are parallel to the plane of tissue section. Depending on the depth of field and focus of an

Table 5 Average modes $m_{near} = \exp(\mu_{near})$ and $m_{far} = \exp(\mu_{far})$ of the two components of the neighborhood distance distribution, broken down by cortical area and diagnosis

Area	m_{near} (μm)		m_{far} (μm)	
	Autistic	Control	Autistic	Control
3	15.2	15.5	25.6	26.1
4	17.3	17.1	27.6	28.9
9	18.1	17.8	27.6	30.4
17	14.9	16.2	22.9	24.1

Within-group standard deviation is 7.1% of the mean

Table 6 Mean nucleolar equivalent radius, i.e. the radius of a circle with area equal to the nucleolar cross section, by diagnosis and cortical area

Area	r_{equiv} (μm)	
	Autistic	Control
3	2.27	3.19
4	2.24	3.08
9	2.56	3.19
17	2.03	2.46

Within-group standard deviation is 0.31 μm

objective, the use of thicker sections allows for a substantial overlap of neighboring minicolumns (see Image capture). The result is a relative diminution in minicolumnar width for both patients and controls when comparing the present study to previous ones [20].

Our initial finding, now corroborated in this study, is that the brains of the autistic patients have minicolumns of reduced width and consequently of increased numbers per linear length of distance [20]. Minicolumnar width varied with cortical area but no other effects were statistically significant. Of the four sampled areas (areas 3, 4, 9, and 17), the dorsolateral prefrontal cortex showed the greatest reduction in minicolumnar width when comparing autistics and controls (Table 2). Since the lateral or granular prefrontal cortex is apparently unique to primates [82], the finding could have important implications regarding putative animal models for autism, especially in rodents. Further topographical inferences regarding a minicolumnopathy in autism would require a larger patient population and a greater number of regions of interest.

The presence of supernumerary minicolumns is said to account for the process of cortical expansion during encephalization [88]. Cortical expansion necessitates an increased number of neurons, but not proportionally [26, 47]. Although the human brain, largely the neocortex, is three times the size of the chimpanzee brain, there is only a 25% increase in the total number of neurons [47]. In our study evidence suggestive of an increased number of minicolumns per linear length in the brains of autistic individuals led us to examine neuronal density. A point process model indicated increased neuronal density but failed to discern the basis for the same, e.g., the presence of supernumerary minicolumns, an increase in the total number of cells per minicolumn, or both. A subsequent analysis based on a Delaunay triangulation addressed the aforementioned possibilities. The new algorithm indicated significant differences in the edges of intercluster distances but not within intracluster distances. Minicolumns appeared to be packed closer together in autism (reduction in far distances) but the total number of cells per minicolumn (near distances) appeared normal. Finally, neurons within the minicolumns of the autistic patients were smaller in size and had a reduction in the size of their nucleoli. In light of the small sample size, the fact that all the various measurements revealed statistically significant differences is surprising. There is a strong possibility, then, that the true effect size associated with some of these measurements is greater than we have observed. Further studies with a larger sample may put tighter bounds on the magnitude of these differences between autistic patients and controls. The following paragraphs discuss the previously mentioned results from the perspective of both neuropathology and possible clinical correlates.

Minicolumns (development and numbers)

Cell arrays are the first radially aligned structure appreciable during development. These modules comprise layer V pyramidal cells (whose dendrites form a bundle extending through layer II), clusters of layer II and III cells, as well as associated interneurons [78]. They have been investigated in a number of species, including barrel field cortex of the mouse [103], barrel field cortex of the rat [75], area 17 of cat [77], visual cortex of non-human primates [14, 76, 78, 79], and various human cortical areas [11, 94, 95]. Pyramidal cell arrays have been the focus of investigation in the studies of columnar development in a series of fetal and adult postmortem tissues. Krmpotić-Nemanić et al. [54] described the development of cell arrays in human fetal and postnatal auditory cortex in a series from celloidin-embedded postmortem material with dates ranging from 9 weeks gestational to 3 months postnatal. They identified continuity in the development of ontogenetic columns into pyramidal arrays with regional differences in the elaboration of the basic columnar structure. Pyramidal cell arrays therefore derive from the ontogenetic cell column and provide the matrix around which growing axonal and dendritic processes are organized. In both monkeys and humans, most of the founder cell divisions that account for the number of cortical columns occur before embryonic day 40 [85, 87]. The genesis for an increase in the total number of minicolumns in autism would therefore transpire at an early stage of gestation.

Minicolumnar size

The possible significance of smaller minicolumns in autistic patients can be gleaned from the results ob-

tained in the comparative studies of columns in cortical area 17 (V1) [31, 74–79]. In primates, the primary visual cortex contains small minicolumns when compared to many other mammals. This is the case even though the brain size of primates is many times greater than the comparison species. Studies using uniformed section thickness in rhesus monkeys have reported minicolumns to be about 23–31 μm on the basis of apical dendrite bundles. By contrast they range from 50 to 60 μm in other small-brained mammals [15, 18]. Researchers have concluded that the narrow minicolumns reflect the increased processing complexity of primate vision and interpreted the smaller minicolumns as being a more complex, interconnected system. In effect, reduced minicolumnar spacing may provide for an increased overlap of their dendritic trees making the function of neighboring minicolumns more interdependent [96, 97].

Cell size and number

Studies estimating cell counts and/or describing cytoarchitectural features in autism have been few in number and have revealed no consistent findings. Aarkrog [1] described ''some cell increase'' in a frontal lobe biopsy. Coleman et al. [28] found significant differences in six out of 42 comparisons when studying the brain of a 21-year-old autistic female and two controls. Kemper and Bauman [52] used qualitative means to describe disturbed lamination in the anterior cingulate gyrus in five out of six autistic patients. No abnormalities in cell counts were reported by Bailey et al. [4] in their six autistic cases. Previous results by Casanova et al. [20] indicate that the brains of autistic patients have smaller and more abundant minicolumns. The tighter packing of cortical modules suggested increased cellular density. A more recent case study examined three cortical areas in nine autistic patients and 11 controls [21]. The overall mean GLI in this series was 19.4% for the control group and 18.7% for the autistic group ($P = 0.724$) with diagnosis-dependent effects in D. The latter authors concluded that in autism a normal GLI and an increased number of modules indicate a reduction in the total number of cells per minicolumn.

In the present study the overall GLI did not differ significantly between autistic patients and controls. The differences in gray level inhomogeneity as described by D and W (Fig. 4) corroborate previous findings that minicolumnar width is reduced in autism [20, 21]. Significant differences in sd_D and sd_W, together with the lack of significant differences in scale-independent variability in minicolumnar width, imply a direct proportionality between the mean and standard deviation of minicolumnar widths within a cortical area.

Instead of cell loss the present study proposes an alternate explanation to the preservation of GLI and increased number of minicolumns: a reduction in neuronal size. Our results indicate the presence of diminished neuronal cell size and increased density in the brains of autistic patients. These findings varied according to brain region (diagnosis by cortical area interaction). The results counter the general notion that, with the exception of striate cortex, cell density is similar across different cortical areas and even among species [90]. The impression of cellular uniformity in cortical columns has been refuted by using modern unbiased techniques [7, 8].

The neurons in our study sample had well-defined nucleoli that were easily distinguishable from other components of the karyoplasm. Histological studies have characterized the nucleolus as an RNA organelle whose function is to regulate protein synthesis. As such the volume of the nucleolus is a constitutional factor adjusted to match the basal metabolic requirements of a cell [66]. The exception to this rule appears to be fast spiking neurons where increased metabolism appears coupled to smaller neuronal size and nucleoli [3]. Pathological conditions causing either increased or decreased cellular activity have an impact on pyramidal cells' nucleolar size in accordance with their protein synthesis requirements [66]. Studies of this and similar morphometric indices have illustrated their utility in conditions such as Alzheimer's disease [64–66] and schizophrenia [29, 61]. In autism a significant diminution in nucleolar size, after thresholding interneurons, suggests a corresponding reduction in the neuronal metabolic activity/efficiency.

Clinical correlates

Brain growth causes the isolation of non-adjacent neurons by expanding their intervening distance. With longer distances the presence of smaller neurons imposes a metabolic constraint on connectivity. Longer connections necessitate larger and more active neurons, where each cell is networked into a dynamically controlled energy system [27, 56]. A cortex biased towards smaller neurons would facilitate signal delays and metabolic inefficiencies when linking disparate brain areas. The result would be reduced or impaired functional connectivity between distant cortical regions [9, 48, 50]. In such a system both sensory coding and motor output, the endpoints of networked chain translating sensory information into behavioral actions,

are normal. It is the intervening step of information analysis that is abnormal.

The presence of smaller neurons in autism may help explain the fact that autism spectrum disorder (ASD) patients normally activate the fusiform gyrus when viewing faces as compared to non-face stimuli [39]. The data indicate that the face-processing deficits encountered in ASD are not due to dysfunction of an individual area, in this case the fusiform gyrus, but due to more complex anomalies in the distributed network of interconnected brain regions [10, 39, 81]. In effect, the level of synchronization during activation tasks involving distant brain regions suggests impaired connectivity in autism [25, 48, 50, 53, 104]. It may be, as Minshew et al. [69] have suggested, that autism is manifested as abnormalities in high-level tasks whenever an elevated demand is placed on information processing [33, 70].

Just et al. [50] have subsumed the evidence for a lower degree of information integration in autism under the rubric of the ''underconnectivity theory.'' However, the term may prove to be a misnomer when applied to shorter intra-areal connections (arcuate or u fibers). In autism, an increase in the total number of minicolumns requires a scale increase (roughly a 3/2 power law) in white matter to maintain modular interconnectivity [46]. This additional white matter takes the form of short-range connections which makes up the bulk of intracortical connections [23]. Recent structural imaging studies suggest that short association fibers are overrepresented in autism [44]. This fact may help explain the superior abilities of the autistic patients when performing tasks that require local information processing [41]. A diminution in neuronal cell size and a concomitant increase in the total number of minicolumns biases cortical connectivity in favor of local rather than global information processing [6]. The result is a ''hyper-specific brain'' [36], where segments of perception are retained at the expense of losing the ''big picture'' [98]. In autism, a computational perspective validates this framework and sees hyperspecificity as a possible framework of neural codes in charge of elaborating concepts [67].

It is noteworthy that an adaptive strategy for increasing the metabolic efficiency of a system driven by smaller neurons is to increase their total cell numbers while reducing the activity of each neuron [60]. This approach, called sparse distributed coding, achieves high representational capacity by distributing small amounts of activity over a large population of neurons [57]. In sparse coding, neurons have the potential to respond strongly to focal features of sensory inputs [32, 40]. Since neurons rarely encounter their feature, they will fire in short bursts, sparingly distributed in time [57]. Sparse-distributed coding is characteristic of the visual system [100, 102]. A brain whose neuronal population is biased towards small neurons and corresponding metabolic exigencies would therefore create and execute strategies that emphasize selective convergence of information among closely adjacent modules, as e.g. in the visual system.

Large system operations can be subdivided into task-specific modules where information processing proceeds along hierarchical stages [49]. Metabolic constraints facilitate the connectivity of closely adjacent cortical areas [35, 68] which represent similar features of perception [93]. The analogy is to an operon where related genes (e.g., coding for enzymes in the same metabolic pathway) cluster together so that outside influences can provide for simultaneous negative or positive control to all of its units. This type of assembly is efficient because perceptions commonly ''overlap with one another, sharing parts which continue unchanged from one moment to another'' [5]. By way of contrast information at higher echelons emphasizes complex conjunctions of perceptual attributes.

When comparing the hierarchy of perceptual networks, primary association cortices, modules become larger and representation more categorical [34, 42]. As a consequence, information at lower echelons of the perceptual hierarchy is more localized and lesions result in concrete deficits. At higher levels, information is more dependent on distributed networks. One good example of a physiological characteristic dependent on a distributed network is face recognition, i.e., nodes in temporal, fusiform, and prepiriform cortex [34]. Another example of greater relevance to autism is joint attention. More so than face processing, multiple studies relate joint attention to diagnosis and outcome in autism [72]. Development of joint attention involves the prefrontal cortical areas 8 and 9 and anterior cingulate area 24. These areas serve to integrate self-monitored information about social intentions with information about goal-related behavior in other people [55] processed in the parietal and temporal lobe. This so-called ''social executive process'' [71] may be especially prone to disturbance wherever an increase in number and proportion of small neurons facilitate the integration of information within a given region while attenuating distal connectivity and coherence.

Acknowledgments We are grateful to the following institutions for the provision of the specimens: Mount Sinai School of Medicine (New York, NY, USA), University of Würzburg Morphological Brain Research Unit (Würzburg, Germany), University of Maryland Brain and Tissue Bank for Develop-

mental Disorders (Baltimore, MD, USA), Harvard Brain Tissue Research Center (Belmont, MA, USA), New York State Institute for Basic Research in Developmental Disabilities (Staten Island, NY, USA) and the US Autism Tissue Program (Princeton, NJ, USA). We thank E.K. Broschk and A. Bahrkel for their technical support. This article is based upon work supported by the Stanley Medical Research Foundation (H.H., C.S., P.R.H. and M.F.C.), the Korczak Foundation (H.v.E.), the National Alliance for Autism Research (C.S. P.R.H. and M.F.C.), the McDonnell Foundation (P.R.H.) and NIMH grants MH61606 (M.F.C.), MH62654 (M.F.C.), MH69991 (M.F.C), NIH MH66392 (P.R.H).

Appendix: Cognitive/functional level of the autistic patients in this study

A1

- Regression at 24 months of age
- Normal or early attainment of all developmental milestones before 2 years of age
- Articulation of 2–3 word sentences with difficulty, echoing
- No spontaneous use of pointing
- Inconsistency in responding to his own name
- Inability to socially greet someone
- No sensitivity to noise
- Stereotypic rather than creative/imaginative play
- Poor eye contact
- No unusual preoccupations or rituals, other than spinning wheels on transportation toys
- Anxiety when routines were changed
- No aggression toward others or himself
- Tantrums
- Sometimes walking on his toes; no spinal problems; very agile
- Age-appropriate growth profile
- No idiosyncratic hand or finger mannerisms
- No neurocutaneous stigmata or musculoskeletal abnormalities
- Immature pencil grip when attempting graphomotor tasks

A2

- Motor milestones met within normal limits; never toilet trained
- Somewhat delayed fine and gross motor skills
- Isolated and withdrawn, in addition to engaging in repetitive behaviors, at 18 months of age
- Language delays
- Lack of speech and low frustration tolerance
- Speech therapy, physical therapy, and occupational therapy
- No consistent use of any words at the age of 5
- No imitation of others' actions or direction of others' attention to things of interest to her
- Qualitative impairments in reciprocal social interaction
- Reduced eye contact and difficulty regulating eye contact in social situations
- Inappropriate facial expressions, such as laughing and crying for no apparent reason
- Occasional engagement in imaginative play by herself; no engagement in imaginative play with others
- Very little interest in other children
- Repetitive play
- Repetitive body movements, such as finger flicking and hand flapping

A3

- Motor milestones were met within normal limits; fully toilet trained
- Use of single words at 18 months of age
- No development of phrase speech by 3 or 4 years of age
- Echoing at 3 years of age, occurring only occasionally by the age of 8
- Poor eye contact between 4 and 5 years of age, with improvement during development
- Speech therapy, physical therapy, and occupational therapy
- Ability to speak in simple sentences, using verbs and other grammatical markings, by 8 years of age
- Difficulty engaging in reciprocal conversation on topics the patient himself introduced
- Difficulty answering direct questions
- Difficulty pronouncing certain words
- Regular use of stereotyped words and phrases
- Difficulty spontaneously imitating the action of others
- Pointing to make requests
- Inattentive to those talking to him
- Well-developed receptive language skills
- Qualitative impairments in reciprocal social interaction
- Inability to express or explain his own pain
- Typical range of facial expressions, but occasionally inappropriate, such as laughing for no apparent reason
- Engagement in some pretend play on his own at the age of 8

- Difficulty engaging in reciprocal social play
- Repetitive play
- Stereotyped whole body movements, such as jumping up and down on his tiptoes
- Extremely affectionate, loving, and kind-hearted
- Well-developed visuospatial skills
- Excellent memory

A4

- Severe hypotonia at 6 months of age
- Ability to sit up without support at 7 months of age
- No walking without support until 4 years of age
- Never toilet trained
- Developmental delays at 29 months of age
- Delays in both fine and gross motor skills
- Physical therapy, occupational therapy, and intensive speech therapy
- Qualitative impairments in communication
- Language delays evident at 15 months of age, using a few single words inconsistently
- Ability to sign a few words learned at about 18 months of age but lost by the age of 4
- Rare spontaneous use of conventional or instrumental gestures between 4 and 5 years of age, only occasional looking up when someone would enter the room without calling patient's name
- Vocalization in the form of jargon and consonant–vowel sounds that were not consistently directed at anyone, at 13 years of age
- Ability to follow only simple directions at 13 years of age
- Rare spontaneous imitation of another person's actions
- Frequent screaming
- Hypersensitivity to certain noises
- Qualitative impairments in reciprocal social interaction
- Ability to make brief make eye contact with familiar adults
- Vocalizing, jumping up and down, and flapping his arms and hands to express excitement
- Struggle to understand emotional experience of others
- Limited range of facial expressions between 4 and 5 years of age, but sufficient by the age of 13 for the patient's parents to understand the major emotions that he experienced, such as happiness, anger, and frustration
- Inappropriate facial expressions, such as laughing for no apparent reason, worsening with age
- No engagement in imaginative play by himself or with others between the ages of 4 and 5, playing next to other children
- Rare interaction with siblings and unresponsiveness to their social approaches or the approaches of less familiar children
- Repetitive play
- Anxiety caused by minor changes in his routine and changes to his immediate environment
- Difficulty processing new environments
- Many unusual sensory interests
- History of aggression towards family members, especially between the ages of 10 and 11, sometimes at school
- Occasional self-injurious behavior, such as head banging
- Affectionate, good natured, and sweet

A5

- Delayed motor milestones
- Delayed language development
- Use of single words, such as ''dog'' and ''hi,'' at approximately 3 years of age
- Ability to speak in short phrases at age 5; no progress beyond spontaneous use of two word combinations; no ability to speak three word phrases spontaneously
- Language regression at age 5 following a grand mal seizure
- Occupational and physical therapy, music and art therapy as well as speech and language, social and life skills training
- No interest in her peers between the ages of 4 and 5
- Qualitative impairments in communication
- Some difficulty coordinating her gaze
- Occasional imitation of noises she had heard; no spontaneous imitation of the actions of others
- No engagement in any form of pretend play
- Qualitative impairments in social interaction
- Difficulty making and maintaining eye contact
- Exceptional visuospatial skill
- Greater interest in certain parts of toys rather than using the toy as it was intended
- No unusual hand or finger mannerisms
- Bouncing up and down while bent over at the waist with arms pulled in tightly to chest to express excitement
- No unusual sensory interests
- Sensitivity to bright lights and excessive noise
- Tactile defensiveness, responding negatively to being touched by others

A6

- Speech delay, rocking, hyperactivity to the point of breaking several playpens, and periodic crying spells at 26 months of age
- Poor eye contact, failure to attend to the breast while feeding, and crying spells as early as 7 months of age (noted retrospectively)
- Independent walking not delayed, noted at 14 months
- No word use until 9 years of age; no phrase use
- Gradual loss of interest of toileting self-care skills
- Disrupted sleeping habits
- Poor eye contact
- Absence of social smiling and limited facial expression
- No imaginative play with others, nor interest in other children
- Absence of shared attention skills
- Lack of empathy
- Use of other's body to communicate
- Laughing for no apparent reason at 4–5 years of age
- No use of any form of gesture to communicate, including pointing and head shaking, and no imitation of others
- Repetitive behaviors including circumscribed interest in listening to music all day, repetitive toy play, insistence on carrying out certain rituals, smelling everything (including non-food items), hand and finger mannerisms, and rocking
- Extreme anxiety with any change in his routine (leading to self-hitting)
- Sound sensitivity, hyperactivity, and aggression toward others (punching)

References

1. Aarkrog T (1968) Organic factors in infantile psychoses and borderline psychoses: retrospective study of 45 cases subjected to pneumoencephalography. Dan Med Bull 15:283–288
2. American Psychiatric Association (2000) Diagnostic and statistical manual of mental disorders, 4th edn. Text rev. APA, Washington
3. Bacci A, Huguenard JR (2006) Enhancement of spike-timing precision by autaptic transmission in neocortical inhibitory interneurons. Neuron 49:119–130
4. Bailey A, Luthert P, Dean A,Harding B, Janota I, Montogomery M, Rutter M, Lantos P (1998) A clinicopathological study of autism. Brain 121:889–905
5. Barlow HB (1972) Single units and sensation: a neuron doctrine for perceptual psychology? Perception 1:371–394
6. Baron-Cohen S (2004) The cognitive neuroscience of autism. J Neurol Neurosurg Psychiatr 75:945–948
7. Beaulieu C, Colonnier M (1989) Number and size of neurons and synapses in the motor cortex of cats raised in different environmental complexities. J Comp Neurol 289:178–181
8. Beaulieu C (1993) Numerical data on neocortical neurons in adult rat, with special references to the GABA population. Brain Res 609:284–292
9. Belmonte MK, Allen G, Belckel-Mitchener A, Boulanger IM, Carper RA, Webb S (2004) Autism and abnormal development of brain connectivity. J Neurosci 24:9228–9231
10. Boddaert N, Zilbovicius M (2002) Functional neuroimaging and childhood autism. Pediatr Radiol 32:1–7
11. Bonin G von, Mehler WR (1971) On columnar arrangement of nerve cells in cerebral cortex. Brain Res 27:1–10
12. Braitenberg V, Schüz A (1998) Cortex: statistics and geometry of neuronal connectivity. Springer, Berlin Heidelberg New York
13. Brodmann K (1909) Vergleichende Lokalisationslehre der Grohhirnrinde. Barth, Leipzig
14. Buxhoeveden DP, Casanova MF (2000) Comparative lateralisation patterns in the language area of human, chimpanzee, and rhesus monkey brains. Laterality 5:315–330
15. Buxhoeveden D, Casanova MF (2002) The minicolumn and evolution of the brain: a review. Brain Behav Evol 60:125–151
16. Buxhoeveden D, Fobbs A, Casanova MF (2002) Quantitative comparison of radial cell columns in developing Down's syndrome and normal cortex. J Intellect Disabil Res 46:76–81
17. Buxhoeveden D, Casanova MF (2004) Accelerated maturation in brains of patients with Down syndrome. J Intellect Disabil Res 48:704–705
18. Buxhoeveden D, Casanova MF (2005) The cell column in comparative anatomy. In: Casanova MF (ed) Neocortical modularity and the cell minicolumn. Nova Biomedical, New York, pp 93–116
19. Carpenter M (1985) Core text of neuroanatomy, 3rd edn. Williams and Wilkins, Baltimore
20. Casanova MF, Buxhoeveden D, Switala A, Roy E (2002) Minicolumnar pathology in autism. Neurology 58:428–432
21. Casanova MF, Buxhoeveden D, Switala A, Roy E (2002) Neuronal density and architecture (gray level index) in the brains of autistic patients. J Child Neurol 17:515–521
22. Casanova MF, Buxhoeveden D, Gomez J (2003) Disruption in the inhibitory architecture of the cell minicolumn: implications for autism. Neuroscientist 9:496–507
23. Casanova MF (2004) White matter volume increase and minicolumns in autism. Ann Neurol 56:453
24. Casanova MF, Switala AE (2005) Minicolumnar morphometry: computerized image analysis. In: Casanova MF (ed) Neocortical modularity and the cell minicolumn. Nova Biomedical, New York, pp 161–180
25. Castelli F, Frith C, Happe F, Frith U (2002) Autism, Asperger syndrome and brain mechanisms for the attribution of mental states to animated shapes. Brain 125:1839–1849
26. Changizi MA (2001) Principles underlying mammalian neocortical scaling. Biol Cybern 84:207–215
27. Chklovskii DB, Koulakov AA (2004) Maps in the brain: what can we learn from them? Annu Rev Neurosci 27:369–392
28. Coleman PD, Romano J, Lapham L, Simon W (1985) Cell counts in cerebral cortex of an autistic patient. J Autism Dev Disord 15:245–255

29. Colon EJ (1972) Quantitative cytoarchitectonics of the human cerebral cortex in schizophrenic dementia. Acta Neuropathol 20:1–10
30. DeFelipe J (1997) Types of neurons, synaptic connections and chemical characteristics of cells immunoreactive for calbindin-D28K, parvalbumin and calretinin in the neocortex. J Chem Neuroanat 14:1–19
31. Feldman ML, Peters A (1974) A study of barrels and pyramidal dendritic clusters in the cerebral cortex. Brain Res 77:55–76
32. Field DJ (1994) What is the goal of sensory coding? Neural Comput 6:559–601
33. Frith C (2004) Is autism a disconnection disorder? Lancet Neurol 3:577
34. Fuster JM (2003) Cortex and mind: unifying cognition. Oxford University Press, Oxford
35. Goodhill GJ (1997) Stimulating issues in cortical map development. Trends Neurosci 20:375–376
36. Grandin T (2005) Animals in translation: using the mysteries of autism to decode animal behavior. Scribner, New York
37. Gressens P, Evrard P (1993) The glial fascicle: an ontogenic and phylogenic unit guiding, supplying and distributing mammalian cortical neurons. Brain Res Dev Brain Res 76:272–277
38. Gupta A, Wang Y, Markram H (2000) Organizing principles for a diversity of GABAergic interneurons and synapses in the neocortex. Science 287:273–278
39. Hadjikhani N, Joseph RM, Snyder J, Chabris CF, Clark J, Steele S, McGrath L, Vangel M, Aharon I, Feczko E, Harris GJ, Tager-Flusberg H (2004) Activation of the fusiform gyrus when individuals with autism spectrum disorder view faces. Neuroimage 22:1141–1150
40. Hahnloser R, Kozhevnikov A, Fee M (2002) An ultrasparse code underlies the generation of neural sequences in a songbird. Nature 419:65–70
41. Happé F (1999) Autism: cognitive deficit or cognitive style? Trends Cogn Sci 3:216–222
42. Hawkins J (2004) On intelligence. Times Books, New York
43. Heinsen H, Heinsen YL (1991) Serial thick, frozen, gallocyanin stained sections of human central nervous system. J Histotechnol 14:167–173
44. Herbert MR, Ziegler DA, Makris N, Filipek PA, Kemper TL, Normandin JJ, Sanders HA, Kennedy DN, Caviness VS Jr (2004) Localization of white matter volume increase in autism and developmental language disorder. Ann Neurol 55:530–540
45. Hofman MA (1985) Neuronal correlates of corticalization in mammals: a theory. J Theor Biol 112:77–95
46. Hofman MA (2001) Brain evolution in hominids: are we at the end of the road? In: Falk D, Gibson KR (eds) Evolutionary anatomy of the primate cerebral cortex. Cambridge University Press, Cambridge, pp 113–127
47. Holloway RL (1968) The evolution of the primate brain: some aspects of quantitative relations. Brain Res 7:121–172
48. Horwitz B, Rumsey JM, Grady CL, Rapoport SI (1988) The cerebral metabolic landscape in autism: intercorrelations of regional glucose utilization. Arch Neurol 45:749–755
49. Hubel DH, Wiesel TN (1962) Receptive fields, binocular interaction and functional architecture of the cat's visual cortex. J Physiol 160:106–154
50. Just MA, Cherkassky VL, Keller TA, Minshew NJ (2004) Cortical activation and synchronization during sentence comprehension in high functioning autism: evidence of underconnectivity. Brain 127:1811–1821
51. Kawaguchi Y, Kubota Y (1997) GABAergic cell subtypes and their synaptic connections in rat frontal cortex. Cereb Cortex 7:476–486
52. Kemper TL, Bauman ML (1993) The contribution of neuropathologic studies to the understanding of autism. Neurol Clin 11:175–187
53. Koshino H, Carpenter P, Minshew N, Cherkassky V, Keller T, Just M (2005) Functional connectivity in an fMRI working memory task in high-functioning autism. Neuroimage 24:810–821
54. Krmpotić-Nemanić J, Kostović I, Nemanić Đ (1984) Prenatal and perinatal development of radial cell columns in the human auditory cortex. Acta Otolaryngol 97:489–495
55. Lau HC, Rogers RD, Haggard P, Passingham RE (2004) Attention to intention. Science 303:1208–1210
56. Laughlin SB, Sejnowski TJ (2003) Communication in neuronal networks. Science 301:1870–1874
57. Laughlin SB (2004) The implications of metabolic energy requirements for the representation of information in neurons. In: Gazzaniga MS (ed) The cognitive neurosciences, 3rd edn. MIT Press, Cambridge, pp 187–196
58. Lega E, Scholl H, Alimi J-M, Bijaoui A, Bury P (1995) A parallel algorithm for structure detection based on wavelet and segmentation analysis. Parallel Comput 21:265–285
59. Letinic K, Zoncu R, Rakic P (2002) Origin of GABAergic neurons in the human neocortex. Nature 417:645–649
60. Levy WB, Baxter RA (1996) Energy-efficient neural codes. Neural Comput 8:531–543
61. Lohr JB, Jeste DV (1986) Cerebellar pathology in schizophrenia? a neuronometric study. Biol Psychiatr 21:865–875
62. Lord C, Rutter M, Le Couteur A (1994) Autism diagnostic interview—revised: a revised version of a diagnostic interview for caregivers of individuals with possible pervasive developmental disorders. J Autism Dev Disord 24:659–685
63. Lord C, Pickles A, McLennan J, Rutter M, Bregman J, Folstein S, Fombonne E, Leboyer M, Minshew N (1997) Diagnosing autism: analyses of data from the autism diagnostic interview [Journal Article. Multicenter Study]. J Autism Dev Dis 27(5):501–517
64. Mann DMA, Yates PO, Barton CM (1977) Cytophotometric mapping of neuronal changes in senile dementia. J Neurol Neurosurg Psychiatry 40:299–302
65. Mann DMA, Sinclair KGA (1978) The quantitative assessment of lipofuscin pigment, cytoplasmic RNA and nucleolar volume in senile dementia. Neuropathol Appl Neurobiol 4:129–135
66. Mann DMA (1982) Nerve cell protein metabolism and degenerative disease. Neuropathol Appl Neurobiol 8:161–176
67. McClelland JL (2000) The basis of hyperspecificity in autism: a preliminary suggestion based on properties of neural nets. J Autism Dev Disord 30:497–502
68. Miller KD (1994) A model for the development of simple cell receptive fields and the ordered arrangement of orientation columns trough activity-dependent competition between ON- and OFF-center inputs. J Neurosci 14:410–416
69. Minshew NJ, Goldstein G, Maurer RG, Bauman ML, Goldman-Rakic PS (1989) The neurobiology of autism: an integrated theory of the clinical and anatomic deficits. J Clin Exp Neuropsychol 11:38
70. Mundy P, Neal AR (2001) Neural plasticity, joint attention, and a transactional social-orienting model of autism. Int Rev Res Ment Retard 23:139–168
71. Mundy P (2003) The neural basis of social impairments in autism: the role of the dorsal medial-frontal cortex and anterior cingulate system. J Child Psychol Psychiatr 44:793–809

72. Mundy P, Burnette C (2005) Joint attention and neurodevelopmental models of autism. In: Volkmar FR, Paul R, Klin A, Cohen D (eds) Handbook of autism and pervasive developmental disorders, 3rd edn. Wiley, New York, pp 650–681
73. Otsu N (1979) A threshold selection method from grey-level histograms. IEEE Trans Syst Man Cybern 9:377–393
74. Peters A, Walsh TM (1972) A study of the organization of apical dendrites in the somatic sensory cortex of the rat. J Comp Neurol 144:253–268
75. Peters A, Kara DA (1987) The neuronal composition of area 17 of rat visual cortex, IV: the organization of pyramidal cells. J Comp Neurol 260:573–590
76. Peters A, Sethares C (1991) Organization of pyramidal neurons in area 17 of monkey visual cortex. J Comp Neurol 306:1–23
77. Peters A, Yilmaz E (1993) Neuronal organization in area 17 of cat visual cortex. Cereb Cortex 3:49–68
78. Peters A, Sethares C (1996) Myelinated axons and the pyramidal cell modules in monkey primary visual cortex. J Comp Neurol 365:232–255
79. Peters A, Sethares C (1997) The organization of double bouquet cells in monkey striate cortex. J Neurocytol 26:779–797
80. Petrides M, Pandya DN (2002) Comparative cytoarchitectonic analysis of the human and the macaque ventrolateral prefrontal cortex and corticocortical connection patterns in the monkey. Eur J Neurosci 16:291–310
81. Pierce K, Haist F, Sedaghat F, Courchesne E (2004) The brain response to personally familiar faces in autism: findings of fusiform activity and beyond. Brain 127:2703–2716
82. Preuss TM (1995) Do rats have a prefrontal cortex? the Rose Woolsey-Akert program reconsidered. J Cogn Neurosci 7:1–24
83. Rajkowska G, Goldman-Rakic PS (1995) Cytoarchitectonic definition of prefrontal areas in the normal human cortex, I: remapping of areas 9 and 46 using quantitative criteria. Cereb Cortex 5:307–322
84. Rajkowska G, Goldman-Rakic PS (1995) Cytoarchitectonic definition of prefrontal areas in the normal human cortex, II: variability in locations of areas 9 and 46 and relationship to the Talairach Coordinate System. Cereb Cortex 5:323–337
85. Rakic P (1974) Neurons in rhesus monkey visual cortex: systematic relation between time of origin and eventual disposition. Science 183:425–427
86. Rakic P (1975) Local circuit neurons. Neurosci Res Prog Bull 13:295–416
87. Rakic P (1985) Limits of neurogenesis in primates. Science 227:1054–1056
88. Rakic P (1995) A small step for the cell, a giant leap for mankind: a hypothesis of neocortical expansion during evolution. Trends Neurosci 18:383–388
89. Rivara CB, Sherwood CC, Bouras C, Hof PR (2003) Stereologic characterization and spatial distribution patterns of Betz cells in the human primary motor cortex. Anat Rec A 270:137–151
90. Rockel AJ, Hiorns RW, Powell TPS (1980) The basic uniformity in structure of the neocortex. Brain 103:221–244
91. Schleicher A, Zilles K (1990) A quantitative approach to cytoarchitectonics: analysis of structural inhomogeneities in nervous tissue using an image analyzer. J Microsc 157:367–381
92. Schleicher A, Palomero-Gallagher N, Morosan P, Eickhoff SB, Kowalski T, Vos K de, Amunts K, Zilles K (2005) Quantitative architectural analysis: a new approach to cortical mapping. Anat Embryol 210:373–386
93. Schwartz EL (1980) Computational anatomy and functional architecture of striate cortex: spatial mapping approach to perceptual coding. Vision Res 20:643–669
94. Seldon HL (1981) Structure of human auditory cortex, I: cytoarchitectonics and dendritic distributions. Brain Res 229:277–294
95. Seldon HL (1981) Structure of human auditory cortex, II: axon distributions and morphological correlates of speech perception. Brain Res 229:295–310
96. Seldon HL (1982) Structure of human auditory cortex, III: statistical analysis of dendritic trees. Brain Res 249:211–221
97. Seldon HL (1985) The anatomy of speech perception: human auditory cortex. In: Jones EG, Peters A (eds) Association and auditory cortices. Plenum, New York, pp 273–327
98. Shakow D (1946) The nature of deterioration in schizophrenic conditions. Coolidge Foundation, New York
99. Stoyan D, Kendall WS, Mecke J (1995) Stochastic geometry and its applications, 2nd edn. Wiley, Chichester
100. Vinje WE, Gallant JL (2000) Sparse coding and decorrelation in primary visual cortex during natural vision. Science 287:1273–1276
101. Vogt C, Vogt O (1919) Allgemeinere Ergebnisse unserer Hirnforschung, dritte Mitteilung: die architektonische Rindenfelderung im Lichte unserer neuesten Forschungen. J Psychol Neurol 25: 361–376
102. Weliky M, Fiser J, Hunt RH, Wagner DN (2003) Coding of natural scenes in primary visual cortex. Neuron 37:703–718
103. White EL, Peters A (1993) Cortical modules in the posteromedial barrel subfield (Sm1) of the mouse. J Comp Neurol 334:86–96
104. Zilbovicius M, Garreau B, Samson Y, Remy P, Barthelemy C, Syrota A, Lelord G (1995) Delayed maturation of the frontal cortex in childhood autism. Am J Psychiatr 152:248–252